Ultracompact Photonic Structure Design for Strong Light Confinement and Coupling Into Nanowaveguide

Mirbek Turduev, Emre Bor, Cagri Latifoglu, Ibrahim Halil Giden, Y. Sinan Hanay, and Hamza Kurt

***Abstract*—Different optimization algorithms have recently been utilized to design and improve the performance of many nanophotonic structures. We present the design of a compact photonic structure by an approach based on machine learning. Three-dimensional finite-difference time-domain method is integrated with a machine learning algorithm in order to design a photonic structure. In particular, a subwavelength focusing lens structure that operates at telecom wavelengths is designed to have desired beam properties such as subwavelength full-width at half-maximum value of 0.155 λ and suppressed side-lobe levels at focal point, where λ denotes the wavelength of incident light and equals to 1550 nm. The designed compact lens structure has the footprint of $2 \times 1\ \mu m^2$ with a slab thickness of 280 nm, which is the smallest photonic lens for subwavelength focusing of light to date comparing to its conventional ones. The focusing mechanism of designed lens structure is explained with the help of applying discrete Fourier transform to the two-dimensional dielectric distribution of the structure. It is also shown that, due to its strong light confinement property, the designed lens structure can be used as a waveguide-to-waveguide optical coupling device with a beamwidth compression ratio of 10:1 by integrating a nanowaveguide with the width of 200 nm to the output surface of lens structure. Normalized transmission efficiency of the optical coupling device is calculated as high as 0.62 at the wavelength of 1550 nm. The outcomes of the presented study show that machine learning can be beneficial for designing efficient compact photonic structures.**

***Index Terms*—Lenses, machine learning algorithms, nanophotonics, photonic integrated circuits.**

I. Introduction

STUDIES on subwavelength light focusing phenomenon are increasing over time due to immense needs of light confinement and concentration into a narrow region [1]–[3]. Light focusing into a tight spot smaller than the wavelength of light may find place in various optical applications including nanolithography, optical microscopy, optical measurements, and optical data storage. In addition, tightly focused light beams can be used in manipulation of nano-particles and objects [4]. Furthermore, super-resolution imaging in subwavelength scale may help to investigate details of cells or very small biological particles such as DNA, viruses, and proteins [5]. Besides of the aforementioned applications, high-resolution imaging and strong beam coupling can also be achieved by using the light focusing effect beyond the diffraction limit of light [6], [7]. Various subwavelength focusing elements have already been developed using metasurfaces [8], plasmonics [9]–[11], metamaterials [12], and all-dielectric materials [13], [14] as well as exploiting super-oscillation [15] and grating lenses [16], [17]. Even though different techniques for achieving subwavelength focusing effect were introduced to literature, they still suffer from important drawbacks such as strong reflection at the interface between host media and focusing device, high material absorption losses due to the imaginary part of the metallic material permittivity, narrowband operation, and stringent material requirements. These drawbacks can affect the focal point resolution that limits the subwavelength focusing performance of the structure. Here, an important question can be raised; how to design an all-dielectric photonic structure exhibiting subwavelength focusing behaviour by avoiding above mentioned problems?

Conventional photonic device design strategies are based on theoretical knowledge and scientific/educational intuitions. However, these approaches may not always fully provide analytical solutions for complex photonic structures and light manipulation behaviour. Furthermore, theoretically designed systems in some cases may not satisfy the performance requirements such as feasibility, compactness, efficiency, bandwidth, and energy transmission. For this reason, a variety of optimization approaches such as evolutionary algorithm [13], inverse optimization [18], topology optimization [19], nonlinear search algorithm [20], and direct binary search algorithm [21] have been implemented to design efficient photonic integrated structures.

In this study, we designed a highly efficient and ultra-compact photonic structure for subwavelength focusing and efficient coupling of light composed of dielectric scatterers by using machine learning approach for the optimization process. Here, machine

Manuscript received December 1, 2017; revised February 24, 2018 and March 27, 2018; accepted March 28, 2018. Date of publication March 30, 2018; date of current version May 31, 2018. This work was supported in part by the Scientific and Technological Research Council of Turkey (TUBITAK) under Grant 116F182 and in part by H. Kurt from the Turkish Academy of Sciences. *(Corresponding author: Mirbek Turduev.)*

M. Turduev and C. Latifoglu are with the TED University, Ankara 06420, Turkey (e-mail: mirbek.turduev@tedu.edu.tr; cagri.latifoglu@tedu.edu.tr; igiden@etu.edu.tr).

E. Bor, I. H. Giden, and H. Kurt are with the TOBB University of Economics and Technology, Ankara 06560, Turkey (e-mail: ebor@etu.edu.tr; hkurt@etu.edu.tr).

Y. S. Hanay is with the Erzurum Technical University, Erzurum 25700, Turkey (e-mail: sinan.hanay@erzurum.edu.tr).

This paper has supplementary downloadable material available at http://ieeexplore.ieee.org. The media file presents visualization of the time evolution of the electric fields and corresponding intensity fields within the designed coupling device at selected wavelengths. The total file size is 14 MB.

Color versions of one or more of the figures in this paper are available online at http://ieeexplore.ieee.org.

Digital Object Identifier 10.1109/JLT.2018.2821361

learning algorithm was implemented for the photonic structure design to reduce the full-width at half-maximum (FWHM) and to suppress the side-lobe levels of the focused light at the focal point. These undesired side lobes occur because of the field scattering at the interface of the structure. In order to have a clear focal plane and large amount of power at the center, these side lobes should be suppressed. Therefore, during the design process, maximum peak value among the side lobes which is defined as the maximum side lobe level (MSLL) value is considered to be minimized. Recently, machine learning has attracted much attention from both academia and industry. Researchers leveraged machine learning successfully in developing a self-learning robot, which can withstand failures [22], improving components' performances in optical communication systems [23], and understanding ecological phenomena [24]. In physics, the machine learning based artificial intelligence has recently been introduced for gravitational wave analysis [25], material designs [26], [27], and phase transitions in quantum physics [28], [29]. In all such diverse examples, the power of machine learning lies in accurate modelling and characterization of complex relationships within the systems. It is important to note that, to the best of authors' knowledge, this is the first time that machine learning approach is utilized to design photonic devices with desired optical properties.

II. Problem Definition and Design Approach

The main purpose of this study is to determine an efficient and ultra-compact photonic structure that exhibits subwavelength focusing effect of the incident light beam. As a criterion of subwavelength focusing effect, the spatial size of the focused beam (FWHM value) should stay under 0.5 λ in air, where λ is wavelength of light. During the design process, one should pay attention to not only the strong light focusing but also to the emergence of side lobes. Because of the strong light scattering at the interface between structure and host medium, the main lobe of the focused beam is generally accompanied with significant side lobes. A large amount of energy shared with side lobes may lead to an undesired radiation pattern, which in turn results in the decreasing of confined energy at the focal point. In other words, if the side lobes of a focal point are reduced, the broadening of the spatial size of the focused beam can be emerged. As a consequence, there is a trade-off between strong focusing of light and controlling side lobe levels. In order to balance such a trade-off, a multi-objective design should be implemented.

In this study, a perceptron-like machine learning algorithm [30] is implemented to obtain subwavelength focusing effect. The algorithm combines the additive updates feature of the perceptron algorithm [31] and the reward for state idea of reinforcement learning [32]. The flowchart of the algorithm is given in Fig. 1. As can be seen from the figure, the machine learning algorithm consists of two phases; training and inference. The training phase starts with creating a photonic structure where scatterers are distributed randomly in space (air). Generated random photonic structure contains 20×10 binary cells (it can also be considered as a 20×10 binary matrix), where high refractive index Si- scatterers are stated as "1" and air cells are

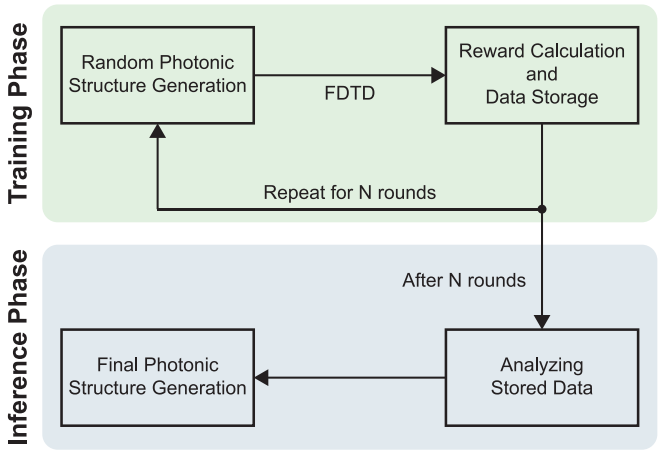

Fig. 1. Flowchart of machine learning based design approach for subwavelength light focusing design.

stated as "0" in the binary matrix. We should note that, before applying the algorithm, we fixed the initial design parameters of binary cells as follows: binary cell is square shaped with sizes of 100 nm $\times$ 100 nm, the height of the cell is 280 nm and the material refractive index is $n_{\mathrm{Si}} = 3.46$. Thus, the size of complete photonic structure equals $2\,\mu$m $\times$ $1\,\mu$m $\times$ $0.28\,\mu$m. It is crucial to note that, the feasibility constraints are considered during design process by incorporating them into the machine learning algorithm where the fixed sizes of binary cells are chosen in accordance to the capability of the state of the art of the fabrication technology [33]. As a second step of the training phase, FDTD method is incorporated to analyze time domain response of the generated photonic structure at an optical telecom wavelength of $\lambda = 1.55\,\mu$m [34]. We should note that in the training phase of the machine learning algorithm, we used freely available MEEP FDTD simulation software on the virtual CPUs of Google Compute Engine. Corresponding FDTD details are explained in the following sections. Especially in time domain responses of the structure, we extracted FWHM and maximum side-lobe levels (MSLL) information of the focused light beam. Here, FWHM and MSLL values are defined as inputs for the reward function R_i of ith randomly generated photonic layout, which is defined as follows:

$$R_i = R_{\max} - (\beta_1 \times F_i + \beta_2 \times S_i) \tag{1}$$

In this expression, F_i and S_i are defined as FWHM and MSLL values of each generated photonic structure, respectively. As can be seen from the objective function, in order to adjust the trade-off between FWHM and MSLL values, weighting factors of β_1 and β_2 are used. Since the objective of the design problem is to find a photonic structure that minimizes both FWHM and MSLL, the reward function R_i approaches to $R_{\max}$. For this reason, the value of constant $R_{\max}$ is arbitrarily chosen by considering the following condition:

$$R_{\max} > (\beta_1 \times F_i + \beta_2 \times S_i) \tag{2}$$

The training phase of machine learning consists of summing the multiplication of binary square matrices and their corre-

sponding rewards. The rewards for each pixel are accumulated in a summation matrix. At the end of training phase, the summation matrix contains the accumulated rewards for each pixel. The inference phase consists of normalizing the summation matrix, and then applying a threshold function to determine the final values for each pixel. Here machine learning takes the mean of the final summation matrix obtained, subtracting this mean from all elements of the matrix, and inferring "1" for a matrix element if the number in that matrix element is positive and "0" if the number is negative, i.e., makes decisions on the final photonic structure that maximizes the given reward function.

In order to explore usefulness of the presented machine learning based design approach, it is important to make a constructive comparison with conventional optimization algorithms. If we consider widely used evolutionary algorithms they heavily depend on the number of generations, diversity of initial solutions and their computational complexity emerges from necessary operations such as reproduction, mutation, recombination, selection and survival of the fittest. All these individual decisions of parameters affect their performance, probabilistic transition and convergence. On the other hand, proposed machine learning algorithm does not require mentioned operations of evolutionary algorithms. Moreover, proposed method is fully parallelizable comparing to iterative optimization approaches. Since random data are generated and evaluated independently from each other, the training process can be divided and distributed arbitrarily to multiple computers which can also lead to avoidance of diversity issues that mainly encountered in optimization algorithms. Moreover, in evolutionary approaches good initial solutions are required for convergence whereas proposed machine learning method does not depend on the quality of initial solutions.

In the presented study, machine learning based design approach is implemented in parallel for FDTD simulations on 12 Google Compute Engine Instances with 2 virtual CPUs and 3.75 GB RAM each. The complete numerical simulations took 72 hours. The number of matrices used in the learning phase (i.e., N rounds) is empirically set to 100000. It is also important to note that in Ref. [35] genetic algorithm (GA) is used for similar objective, i.e., focusing and coupling photonic device design. If one compares the efficiency of proposed machine learning algorithm with applied GA approach in Ref. [35], to achieve the defined objective GA approach required 500000 runs and the complete simulations took 30 days. Therefore, one can deduce that machine learning approach can accomplish the similar task with requiring less number of simulation runs which reduces the total computational time of design process.

III. Numerical Results and Discussion

The designed photonic structure consists of square dielectric Si-cells that intelligently distributed in an air medium, i.e., machine learning algorithm determines the locations of dielectric cells to obtain the desired focusing effect in the optical near-field. A crucial point of the machine learning algorithm is to determine photonic structure that is capable of strong light focusing for transverse-magnetic (TM) polarization, where the magnetic field is along the *xy*-plane (H_x,H_y) and the electric field E_z is perpendicular to the *xy*-plane. Here, the selection of polarization is not limited to TM and transverse-electric (TE) polarization can also be implemented in a similar way. Commercially available software Lumerical FDTD Solutions is used to analyse the subwavelength focusing efficiency of designed focusing device in three-dimensional (3D) spatial domain [36]. The same software is employed to investigate the effect of slab thickness on performance of inferred/designed focusing structure and to calculate the coupling efficiency of proposed optical coupling structure in the following sections of the study.

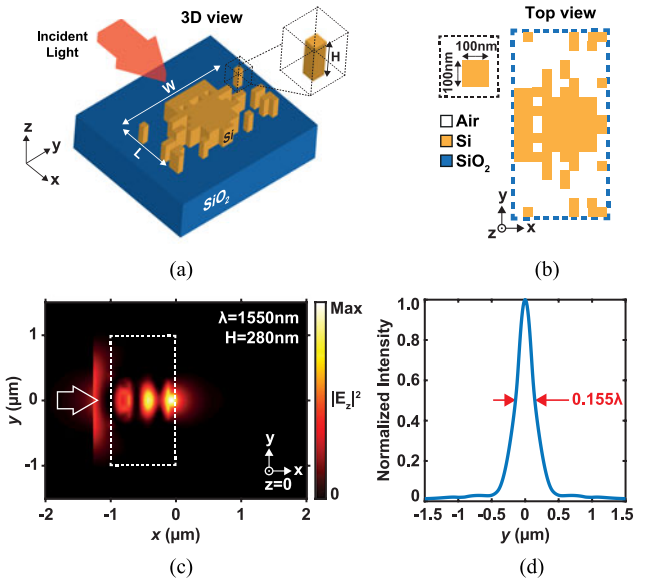

Fig. 2. (a) 3D and (b) top view representations of the designed binary photonic structure with its structural parameters. (c) Spatial intensity distribution at $z = 0$ plane for the designed photonic structure that is indicated by a dashed region. (d) Lateral cross-section of normalized intensity distribution at the focal point of designed photonic structure that has the ability of subwavelength focusing of light with FWHM value of 0.155 λ.

In order to eliminate the undesired back reflections, the boundaries of the computational domain are surrounded by perfectly matched layers. Generated photonic structures are excited via TM polarized continuous source at the design frequency to extract corresponding steady-state spatial intensity distribution. It is important to note that in all numerical calculations, the Gaussian profiled light source is employed to excite the structure, i.e., the amplitude of the source is multiplied by a spatial Gaussian function to account for a finite and smooth beam width. Since the aim of this study is to design a subwavelength focusing photonic device for optical communication applications, the design wavelength is fixed to an optical telecom wavelength of 1550 nm. The best performance of subwavelength focusing, i.e., the structure with maximum reward value, is obtained for the configuration given in Fig. 2(a). The designed photonic lens was constructed on a silicon-on-insulator (SOI) substrate with top silicon thickness of 280 nm and an oxide thickness of 3.5 μm. The Si- slab and SiO_2 substrate refractive indices are fixed to $n_{\mathrm{Si}} = 3.46$ and $n_{SiO2} = 1.44$, respectively.

In Fig. 2(a) and (b), we represent the 3D and top view of the designed lens with corresponding structural parameters,

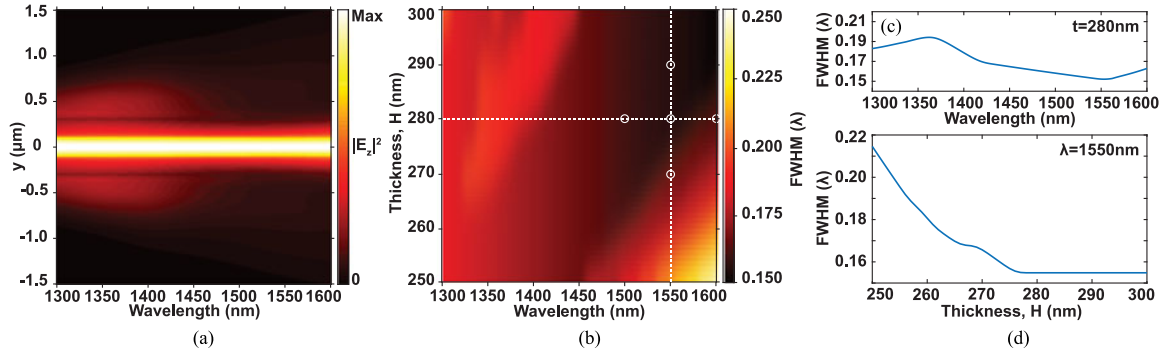

Fig. 3. (a) Normalized transverse cross-section intensity map at the focal point for different operating wavelengths ranging from 1300 nm to 1600 nm of incident light at constant thickness of 280 nm. (b) Map of calculated FWHM values at different thickness of the designed lens for specified wavelength spectrum. (c) Calculated FWHM values of the designed lens at specified spectrum for constant thickness of 280 nm. (d) Calculated FWHM of the lens operating at 1550 nm for different values of thickness.

respectively. The width and length of photonic lens are equal to $\{W,\ L\} = \{2\,\mu\text{m}, 1\,\mu\text{m}\}$, respectively, and to be compatible with SOI technology and optical communication systems, the slab thickness of the designed structure is fixed to $H = 280\,\text{nm}$ throughout the design process. As can be deduced from the view of the photonic lens, during the design process to obtain focal point along the optical axis, each generated structure is arranged to be mirror-symmetrical along the propagation x-axis. Fig. 2(c) represents the steady-state field intensity distribution of the designed photonic lens. As can be seen from the plot, light localized along the optical center of the structure and exits the structure with small focal spot size at the incident wavelength of 1550 nm. The focal point is at the output edge of the designed structure that produces a near-field focusing. Moreover, it can be concluded from the same plot that very poor back reflections occur at the input plane of the structure. Here, the intensity field distribution is extracted at $z = 0$, xy cross-sectional plane and the focusing property of the designed structure is investigated at only $z = 0$ plane, i.e., the focal point is elongated along z-direction which implies a line-focusing. Corresponding transverse cross-section of intensity distribution at focal point is represented in Fig. 2(d). As a demonstration of sub-wavelength focusing, FWHM value of the designed lens is calculated as 0.155 λ (240.25 nm) for the wavelength of incident light of 1550 nm.

In order to show the broadband subwavelength focusing effect of the designed photonic lens, corresponding transverse cross-sections of output electric field intensities were calculated for various incident wavelengths ranging between 1450 nm and 1600 nm and superimposed in Fig. 3(a) as a transverse cross-sectional intensity map, in which case the slab thickness H of the structure is fixed to be 280 nm and a broadband Gaussian source is incident to the structure with the wavelengths covering 1300 nm–1600 nm range. Fig. 3(a) shows that the strong concentration of exiting beam occurs at the lateral cross-section ($y = 0$) at focal point with a small amount of power residing around the optical axis, i.e., x-axis, due to existing side lobes. It should be noted that, while dealing with the strong light focusing effect, it is crucial to consider the emergence of side lobes. Excessive side lobe radiations cause the reduction of the main lobe which is undesirable for strong light focusing. Therefore, a main purpose of using machine learning is to suppress the intensity levels of the MSLLs besides of minimizing the FWHM values at the focal point. It can be clearly observed in the Figs. 2(c) and Fig. 3(a) that incident beam is concentrated into a narrower spot with almost negligible levels of additional undesired side lobes.

It is also necessary to inspect the focusing performance of the structure for variation of slab thickness. Therefore, the slab thickness H of the structure is varied in the range from 250 nm to 300 nm and FWHM values are calculated behind the output surface of the designed structure. The collected results are given as a map of FWHM values with respect to the variations of slab thicknesses H and the incident wavelengths with TM polarization in Fig. 3(b). As can be seen from the map that the cross-section of dashed lines indicates the predefined thickness value of 280 nm and wavelength of 1550 nm, which are the parameters fixed during the design process. The intensities of the map indicate the FWHM values for slab thickness changing from 250 nm to 300 nm fluctuating between 0.14 λ and 0.26 λ. It means that, even for possible variation in the thickness between 250 nm and 300 nm, the designed photonic lens still performs the desired subwavelength focusing effect.

In order to investigate the focusing performance quantitatively, we extracted vertical and horizontal cross-sectional data from the map given in Fig. 3(a) and plotted the results in Fig. 3(c) and (d), respectively. Here, the curve in Fig. 3(c) represents the variation of FWHM values according to the operating wavelength. On the other hand, Fig. 3(d) shows the FWHM variation due to photonic slab thickness change. As indicated in Fig. 3(c) and (d), the calculated FWHM values stays below 0.16 λ for the wavelengths between 1450 nm and 1590 nm at constant thickness of 280 nm and the thickness values between 275 nm and 300 nm are sufficient for obtaining FWHM value of 0.16 λ for wavelength of 1550 nm.

The remarkable features of the designed lens structure can be investigated in detail. For this reason, we considered the different wavelengths and slab thickness values for the designed lens structure. As can be seen from the map given in Fig. 3(b), white circles except the cross sections of dashed lines indicate the selected operating wavelengths and slab thickness values. Firstly, the broadband operating property of the designed lens with slab

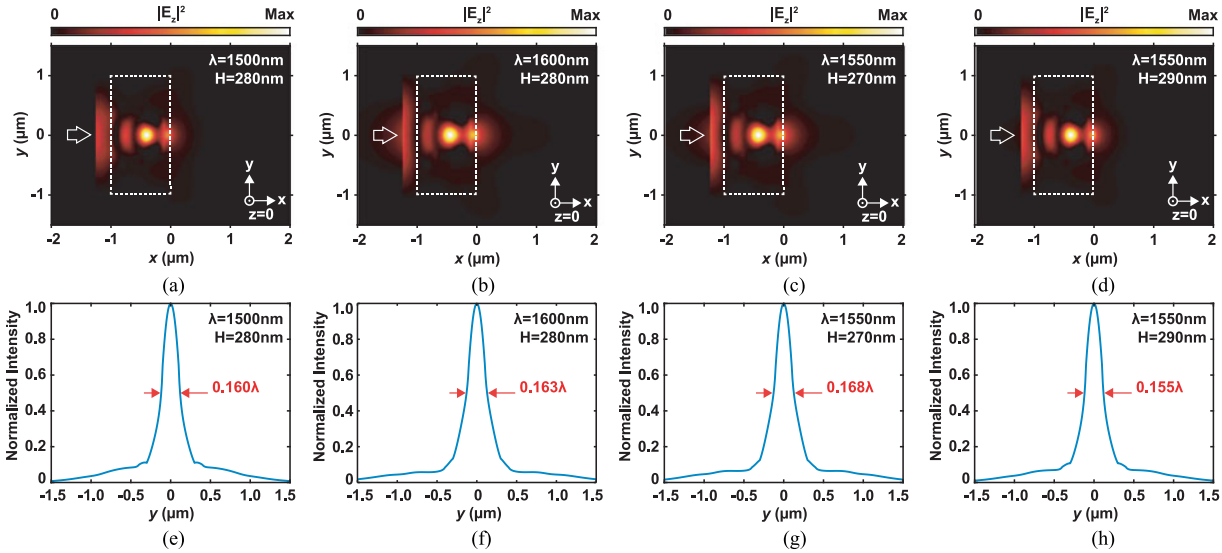

Fig. 4. Intensity distributions and intensity cross-sections at focal points for different wavelengths of incidence and slab thicknesses are represented. Intensity distributions of the structure with slab thickness of 280 nm for operating wavelengths of 1500 nm and 1600 nm are given in (a) and (b), respectively. Intensity distributions of the structure with different slab thicknesses of 270 nm and 290 nm at operating wavelength of 1550 nm are given in (c) and (d), respectively. Intensity cross-sections at focal points of structure with selected operating wavelengths and slab thicknesses in (a), (b), (c) and (d) are given in (e), (f), (g) and (h), respectively.

thickness of 280 nm is examined at the wavelengths of incidence of 1500 nm and 1600 nm and the corresponding intensity distributions for selected wavelengths are given in Fig. 4(a) and (b), respectively. Intensity cross-sections for these cases are given in Fig. 4(e) and (f). As it is seen from these figures, the calculated FWHM values are still around the 0.16 λ which means that the subwavelength focusing can be obtained for a broad wavelength interval of 100 nm. Another important property to consider for integrable photonic structures is the slab thickness that may be uncertain due to the fabrication errors. For this purpose, we consider the slab thickness values of 270 nm and 290 nm for the designed lens structure operating at 1550 nm and the intensity distributions of the selected slab thicknesses are given in Fig. 4(c) and (d), respectively. Intensity cross-sections at focal points for the corresponding intensity distributions are represented in Fig. 4(g) and (h). As can be seen from these figures, the calculated FWHM values are smaller than 0.17 λ. Thus, we can infer that the designed lens structure is robust to the variable slab thickness values.

It is important to give an insight to the physical background of strong light focusing effect of the designed structure. The distribution of the Fourier components in reciprocal space can give insights to the light-matter interaction behavior and the modal (diffraction modes) properties of the structure [19], [37]. For this reason, we performed two-dimensional (2D) discrete Fourier transformation (DFT) of the designed photonic structure to examine optical scattering properties of a designed structure. The 2D DFT can be expressed mathematically by following equation:

$$F(k_x, k_y) = \sum_{x=0}^{M-1} \sum_{y=0}^{N-1} \varepsilon(x, y)\, e^{-j2\pi\left(\frac{k_x x}{M} + \frac{k_y y}{N}\right)}, \qquad (3)$$

where $\varepsilon(x,y)$ is a permittivity of a dielectric medium of size M×N as a function of a position in xy-plane. To better understand the spatial spectrum of the Fourier transform, we compared the designed structure with other randomly distributed mirror symmetric and non-symmetric structures and summarized the results in Fig. 5. This figure represents the designed structure (left); the intensity field distribution at the incident wavelength of 1550 nm (center) and corresponding Fourier transform of the designed structure (right), which indicates the reciprocal space distribution of the propagating modes and the white arrow in Fig. 5(a) (right) indicates the direction of incident wavevector $\boldsymbol{k}_{\text{in}}$. As can be seen from the Fourier spectrum, distributed Si-cells in the designed photonic lens yields wavevectors that are collected in a central area denoted by the red circles. These substantially compressed wavevectors correspond to modes that are confined in the structure. Moreover, different modes exist nearby to the central speckle in the Fourier spectrum depending on the different discrete index distribution of the designed structure. The incident light with $\boldsymbol{k}_{\text{in}}$ excites different modes with $\boldsymbol{k}_{\text{x}}$ and $\boldsymbol{k}_{\text{y}}$ wave vector components. We assume that the propagation direction is x-axis, and then fundamental mode corresponds to small $\boldsymbol{k}_{\text{y}}$ terms. In the case of the optimized photonic structure, for example, mainly the fundamental mode is excited with large $\boldsymbol{k}_{\text{x}}$ component. However, in the cases of photonic structures where Si- randomly distributed Fourier domain patterns exhibit dispersed wavevectors of diffraction orders as shown in Fig. 5(b) (right) and 5(c) (right). Therefore, one can conclude that incident wave energy is transferred to different diffraction modes, resulting in power dissipation inside the structure so that an inefficient light confinement occurs at the output surface of the structure, see the corresponding field intensity distributions in Fig. 5(b) (center) and 5(c) (center). We can also imply that these diffused speckles in Fourier spectra correspond to other higher-order diffraction modes that weaken the power of

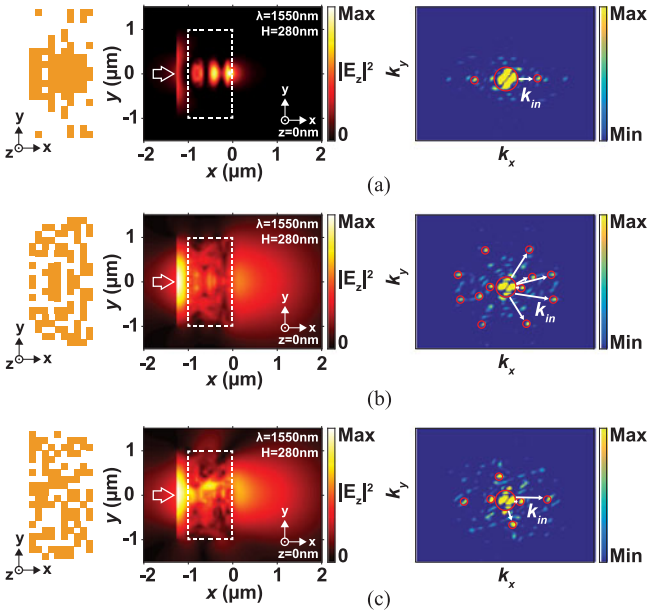

Fig. 5. (a) Left: Designed photonic structure with highest reward value; Center: The intensity distribution at 1550 nm operating wavelength; Right: Corresponding reciprocal space representation of the structure. (b) Left: Randomly generated mirror symmetric photonic structure with lowest reward value; Center: Intensity distribution at 1550 nm operating wavelength; Right: Corresponding reciprocal space representation of the structure. (c) Left: Randomly generated non-symmetric photonic structure; Center: Intensity distribution at 1550 nm operating wavelength; Right: Corresponding reciprocal space representation of the structure. White arrows that are given as insets indicate direction of incident wavevectors.

directional propagation. As a result, we can say that the designed photonic structure via the machine learning algorithm provides strong light confinement with subwavelength focusing effect and is able to efficiently transfer the light to the output space.

The above presented results show that the designed structure provides a broadband sub-wavelength focusing effect under $\lambda/6.25$ within the optical telecom wavelengths. Such a strong subwavelength focusing property can be used in integrated photonic systems to confine light from wider to narrower optical waveguide. Here, the important role of coupling region should be squeezing down of propagating spatial field profile to match to the width of the narrow waveguide. In addition to strong light confinement behavior, the small footprint size as well as the corresponding Fourier transform as in Fig. 5(a) demonstrates that indeed the designed photonic lens can be considered as an alternative and promising solution for waveguide-to-waveguide optical coupling applications. Furthermore, the designed structure is all-dielectric so that such a photonic device is free of absorption losses and it may operate in a broadband regime comparing to its plasmonic and metamaterial counterparts [9], [12].

The coupling effect is also investigated in detail in the study using the proposed machine learning based photonic lens. For this reason, Si- bulk waveguide with the width of 200 nm is butt-coupled to the back surface of the structure [38]. As an input waveguide, Si- bulk material with the width of 2 μm is integrated to the front surface of the structure. 3D representation of the designed waveguide-to-waveguide coupler with thickness of 280 nm and corresponding top view of it are given in Fig. 6(a) and (b), respectively. Transmission efficiency of the designed coupling structure is calculated between wavelengths of 1300 nm and 1600 nm, and shown in Fig. 6(c). In this figure, dashed lines indicate the wavelengths of 1550 nm, 1322 nm and 1419 nm as design wavelength, wavelength of maximum transmission and wavelength of minimum transmission, respectively. The transmission efficiency for wavelength of 1550 nm is calculated as 62%. Maximum transmission value is calculated as 72% at wavelength of 1322 nm. Minimum transmission value is calculated as 51% at wavelength of 1419nm. It is important to note that, during the transmission efficiency calculations via 3D FDTD analyses, the coupling losses as well as out-of-plane-losses in z-plane are considered.

In order to show and compare coupling performances of conventional couplers with proposed design, we have numerically analysed two different coupling mechanisms such as butt- and adiabatic tapered couplings. Corresponding coupling efficiencies of butt- and adiabatic tapered couplers having exact same coupling region dimensions are depicted in Fig. 6(c) with dashed and dash dotted plots, respectively. As can be seen from Fig. 6(c), for the but-coupling mechanism the coupling efficiency between operating wavelengths of 1300 nm and 1600 nm fluctuates between 20% and 35% whereas slightly higher efficiency for the tapered coupler can be observed in a same figure plot. Low transmission appears because of strong back reflections and undesired diffractions that occur when the incident light strikes the junction region (the edge interface between butt-coupler and output waveguide). Moreover, a large portion of field leakage into the free-space occurs at the waveguide junction interface. In the case of tapered coupler, the amount of back-reflection and light leakage at the interface is slightly reduced because of tapered region. In order to achieve higher coupling efficiency, the length of the tapered region should be considerably enlarged to match coupling to radiation modes which is not desirable for on-chip optical applications. The exact value of coupling efficiency at operating telecom wavelength of $\lambda = 1550$ nm for butt-, adiabatic and designed couplers are calculated as 21%, 27% and 62%, respectively.

It can be deduced from these results that the designed structure can be implemented for efficient waveguide-to-waveguide light coupling application with the incident beam compression ratio of 10:1. In other words, the designed coupler transfers light energy from 2 μm width waveguide to 200 nm waveguide with 62% coupling efficiency at telecom wavelength of 1550 nm (wavelength of subwavelength photonic lens design). Moreover, the designed coupler still exhibits a reasonable coupling performance above 51% within the broad wavelength range from 1300 nm to 1600 nm.

Corresponding steady state electric field (E_z) distributions for the wavelengths of 1550 nm, 1322 nm and 1419 nm are given in Fig. 7(a)–(c), respectively. Field distributions in different regions (input, coupler, and output) can be observed from the plots at selected representative wavelengths. Spatial electric field intensity distributions for the same wavelengths are also shown in Fig. 7(d)–(f). In these figures, the dashed lines

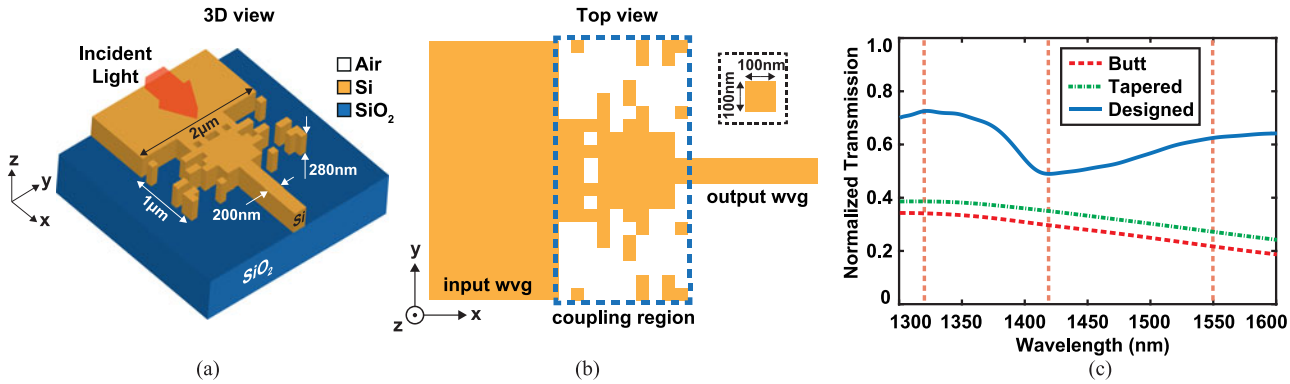

Fig. 6. (a) 3D and (b) top view representations of the designed waveguide-to-waveguide coupler with its structural sizes. (c) Calculated coupling efficiencies of butt- (dashed line), tapered (dash dotted line) and designed (solid line) couplers.

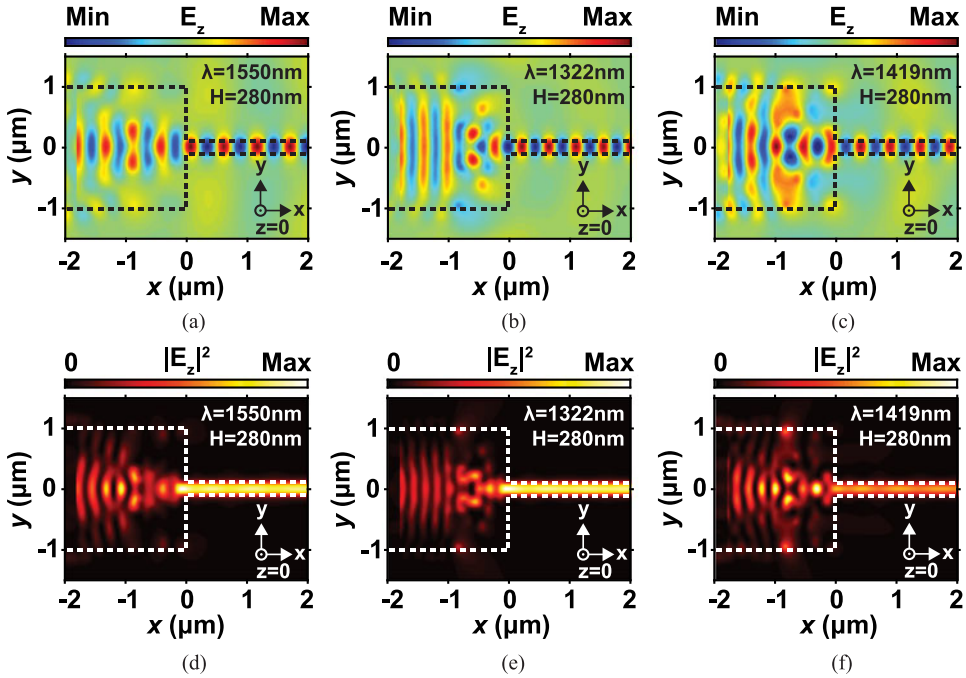

Fig. 7. Steady-state spatial electric-field distributions of designed coupler at $z = 0$ plane for incident wavelengths of 1550 nm, 1322 nm and 1419 nm is represented in (a), (b) and (c), respectively. Spatial field intensity distributions of designed coupler at $z = 0$ plane for incident wavelengths of 1550 nm, 1322 nm and 1419 nm is represented in (d), (e) and (f), respectively. The dashed boxes represent the structural boundaries.

represent the boundaries of designed coupling structure. In order to visualize the time evolution of the electric fields and corresponding intensity fields within the designed coupling device at selected wavelengths, we prepared animation and included it as supplementary information in Media 1. By looking at the intensity profiles in Fig. 7, one important fact should be concluded: a strong modal match occurs at the output waveguide which improves the single mode coupling efficiency of the proposed coupler design. Considering the coupling efficiency in Fig. 6(c), it can be concluded that the designed lens structure performs a tolerable coupling effect. Such efficient single mode coupling efficiency will inevitably render the proposed structure undesirable for single-mode integrated photonics applications.

IV. Conclusion

We introduce the design of subwavelength focusing lens by a machine learning algorithm and numerically investigate its subwavelength focusing property at optical telecom wavelengths by using 3D FDTD method. The designed lens structure has the strong focusing ability with the FWHM of 0.155 λ and repressed side-lobe levels. For operating wavelength interval between 1500 nm and 1600 nm and slab thickness values between 270 nm and 300 nm, FWHM are calculated at around λ/6 which indicates that the designed structure has broadband operating bandwidth of 6.45% and robust to the unsteady slab thickness due to possible fabrication errors. The discrete Fourier transform is utilized to explain the physical background of focusing mechanism of the designed lens structure. Moreover, a possible

application of designed lens structure as an optical coupling device is presented. The calculated transmission efficiency of coupling device is 62% at the wavelength of 1550 nm. The designed coupling structure has compression ratio of 10:1 and shows coupling efficiency above 51% between wavelength interval of 1300 nm and 1600 nm (bandwidth of 20.68%). Alongside their compactness, the designed photonic structures are all-dielectric, feasible for SOI technology and preferable in photonic integrated circuits. As a concluding remark, machine learning algorithm can be considered as a powerful tool to design efficient and compact photonic integrated structures.

REFERENCES

[1] E. Betzig, J. K. Trautman, T. D. Harris, J. S. Weiner, and R. L. Kostelak, "Breaking the diffraction barrier: Optical microscopy on a nanometric scale," *Science*, vol. 251, no. 5000, pp. 1468–1470, Mar. 1991.

[2] J. B. Pendry, "Negative refraction makes a perfect lens," *Phys. Rev. Lett.*, vol. 85, no. 18, pp. 3966–3969, Oct. 2000.

[3] N. Fang, H. Lee, C. Sun, and X. Zhang, "Sub-diffraction-limited optical imaging with a silver superlens," *Science*, vol. 308, no. 5721, pp. 534–537, Apr. 2005.

[4] D. Gao *et al.*, "Optical manipulation from the microscale to the nanoscale: Fundamentals, advances, and prospects," *Light Sci. Appl.*, vol. 6, p. e17039 (1-15), Sep. 2017.

[5] R. F. Laine1, A. Albecka, S. van de Linde, E. J. Rees, C. M. Crump, and C. F. Kaminski, "Structural analysis of herpes simplex virus by optical super-resolution imaging," *Nature Commun.*, vol. 6, Jan. 2015, Art no. 5980.

[6] Z. Jacob, L. V. Alekseyev, and E. Narimanov, "Optical hyperlens: Far-field imaging beyond the diffraction limit," *Opt. Express*, vol. 14, no. 18, pp. 8247–8256, Aug. 2006.

[7] A. Poddubny, I. Iorsh, P. Belov, and Y. Kivshar, "Hyperbolic metamaterials," *Nature Photon.*, vol. 7, no. 12, pp. 948–957, Nov. 2013.

[8] N. Yu and F. Capasso, "Flat optics with designer metasurfaces," *Nature Mater.*, vol. 13, no. 2, pp. 139–150, Jan. 2014.

[9] F. Ye, D. Mihalache, B. Hu, and N. C. Panoiu, "Subwavelength vertical plasmonic lattice solitons," *Opt. Lett.*, vol. 36, no. 7, pp. 1179–1181, Apr. 2011.

[10] H. Li *et al.*, "Enhanced focusing properties using surface plasmon multilayer gratings," *IEEE Photon. J.*, vol. 4, no. 1, pp. 57–64, Feb. 2012.

[11] S. Jia, Y. Wu, X. Wang, and N. Wang, "A subwavelength focusing structure composite of nanoscale metallic slits array with patterned dielectric substrate," *IEEE Photon. J.*, vol. 6, no. 1, Feb. 2014, Art no. 4800108.

[12] A. Kannegulla and L. Cheng, "Subwavelength focusing of terahertz waves in silicon hyperbolic metamaterials," *Opt. Lett.*, vol. 41, no. 15, pp. 3539–3542, Aug. 2016.

[13] E. Bor, M. Turduev, and H. Kurt, "Differential evolution algorithm based photonic structure design: Numerical and experimental verification of subwavelength $\lambda/5$ focusing of light," *Sci. Rep.*, vol. 6, Aug. 2016, Art no. 30871.

[14] M. Turduev, Z. Hayran, and H. Kurt, "Focusing of light beyond the diffraction limit by randomly distributed graded index photonic medium," *J. Appl. Phys.*, vol. 120, no. 24, Dec. 2016, Art no. 243102.

[15] F. M. Huang and N. I. Zheludev, "Super-resolution without evanescent waves," *Nano Lett.*, vol. 9, no. 3, pp. 1249–1254, Jan. 2009.

[16] S. Thongrattanasiri and V. A. Podolskiy, "Hypergratings: Nanophotonics in planar anisotropic metamaterials," *Opt. Lett.*, vol. 34, no. 7, pp. 890–892, Apr. 2009.

[17] S. Vo *et al.*, "Sub-wavelength grating lenses with a twist," *IEEE Photon. Technol. Lett.*, vol. 26, no. 13, pp. 1375–1378, May 2014.

[18] J. Lu and J. Vuckovic, "Nanophotonic computational design," *Opt. Express*, vol. 21, no. 11, pp. 13351–13367, Jun. 2013.

[19] P. Borel *et al.*, "Topology optimization and fabrication of photonic crystal structures," *Opt. Express*, vol. 12, no. 9, pp. 1996–2001, May 2004.

[20] B. Shen, P. Wang, R. Polson, and R. Menon, "Integrated metamaterials for efficient and compact free-space-to-waveguide coupling," *Opt. Express*, vol. 22, no. 22, pp. 27175–27182, Nov. 2014.

[21] B. Shen, R. Polson, and R. Menon, "Integrated digital metamaterials enables ultra-compact optical diodes," *Opt. Express*, vol. 23, no. 8, pp. 10847–10855, Apr. 2015.

[22] A. Cully, J. Clune, D. Tarapore, and J. B. Mouret, "Robots that can adapt like animals," *Nature*, vol. 521, no. 7553, pp. 503–507, May 2015.

[23] D. Zibar, M. Piels, R. Jones, and C. G. Schaeffer, "Machine learning techniques in optical communication," *J. Lightw. Technol.*, vol. 34, no. 6, pp. 1442–1452, Mar. 2016.

[24] J. D. Olden, J. J. Lawler, and N. L. Poff, "Machine learning methods without tears: A primer for ecologists," *Quart. Rev. Biol.*, vol. 83, no. 2, pp. 171–193, Jun. 2008.

[25] R. Biswas *et al.*, "Application of machine learning algorithms to the study of noise artifacts in gravitational-wave data," *Phys. Rev. D*, vol. 88, no. 6, Sep. 2013, Art no. 062003.

[26] S. V. Kalinin, B. G. Sumpter, and R. K. Archibald, "Big-deep smart data in imaging for guiding materials design," *Nature Mater.*, vol. 14, no. 10, pp. 973–980, Sep. 2015.

[27] J. Carrasquilla and R. G. Melko, "Machine learning phases of matter," *Nature Phys.*, vol. 13, pp. 431–434, Feb. 2017.

[28] L. Wang, "Discovering phase transitions with unsupervised learning," *Phys. Rev. B*, vol. 94, no. 19, Nov. 2016, Art no. 195105.

[29] D. Deng, X. Li, and S. Das Sarma, "Machine learning topological states," *Phys. Rev. B*, vol. 96, no. 19, Nov. 2017, Art no. 195145.

[30] C. Latifoglu, "Binary matrix guessing problem," Jan. 2017. [Online]. Available: arXiv: e-prints, vol.1701.06167

[31] F. Rosenblatt, "The perceptron: A probabilistic model for information storage and organization in the brain," *Psychological Rev.*, vol. 65, no. 6, pp. 386–408, 1958.

[32] R. S. Sutton and A. G. Barto, *Introduction to Reinforcement Learning*. Cambridge, MA, USA: MIT Press, 1998.

[33] A. Majumder, B. Shen, R. Polson, and R. Menon, "Ultra-compact polarization rotation in integrated silicon photonics using digital metamaterials," *Opt. Express*, vol. 25, no. 17, pp. 19721–19731, Aug. 2017.

[34] A. F. Oskooi, D. Roundy, M. Ibanescu, P. Bermel, J. D. Joannopoulos, and S. G. Johnson, "Meep: A flexible free-software package for electromagnetic simulations by the FDTD method," *Comput. Phys. Commun.*, vol. 181, no. 3, pp. 687–702, Mar. 2010.

[35] A. Hakanson, J. Sanchez-Dehesa, and L. Sanchis, "Inverse design of photonic crystal devices," *IEEE J. Sel. Areas Commun.*, vol. 23, no. 7, pp. 1365–1371, Jul. 2005.

[36] Lumerical Inc. [Online]. Available: http://www.lumerical.com/tcad-products/fdtd/. Accessed Dec. 2017.

[37] C. Wang, S. Yu, W. Chen, and C. Sun, "Highly efficient light-trapping structure design inspired by natural evolution", *Sci. Rep.*, vol. 3, Jan. 2013, Art no. 1025.

[38] J. B. Driscoll, R. M. Osgood, R. R. Grote, J. I. Dadap, and N. C. Panoiu, "Squeezing light in wires: Fundamental optical properties of Si nanowire waveguides," *J. Lightwave Technol.*, vol. 33, no. 14, pp. 3116–3131, Jul. 2015.

Authors' biographies not available at the time of publication.